



Demonstration of enhanced direct-drive implosion efficiency using gradient pulsesHao Liu ^{1,4}, Xiaohu Yang ^{2,4}, Yihang Zhang,³ Yuan Fang,^{1,4} Zhe Zhang,^{3,4} Xiaohui Yuan,^{1,4} Yutong Li,^{3,4} and Jie Zhang^{1,3,4,*}¹Key Laboratory for Laser Plasmas (MoE), School of Physics and Astronomy, Shanghai Jiao Tong University, Shanghai 200240, China²Department of Physics, National University of Defense Technology, Changsha 410073, China³Beijing National Laboratory for Condensed Matter Physics, Institute of Physics, Chinese Academy of Sciences, Beijing 100190, China⁴Collaborative Innovation Centre of IFSA, Shanghai Jiao Tong University, Shanghai 200240, China

(Received 20 December 2021; revised 24 March 2022; accepted 12 May 2022; published 31 May 2022)

Higher implosion efficiency is of great significance in direct-drive fusion research. We demonstrated the critical role played by the intensity gradient of the main drive laser pulse in improving efficiency of direct-drive implosions, using a double-gradient nanosecond pulse. Compared with a square pulse, the burn-through depth was increased by over 200%, and the shell velocity was increased by ~ 2.1 times with an optimized double-gradient pulse. As the result, the implosion efficiency was enhanced by \sim six times. It was found that by limiting the intensity gradient of the main drive pulse to no more than $\sim 2.5 \times 10^{15}$ W/(cm²ns), heat flux inhibition by nonlocal electron thermal transport effects could be eliminated, and ultimately an efficient mass ablation process was achieved. These results have relevance for pulse designs in ignition-scale direct-drive implosions.

DOI: [10.1103/PhysRevE.105.L053203](https://doi.org/10.1103/PhysRevE.105.L053203)

In direct-drive inertial confinement fusion (ICF) [1], after the laser beams propagate through a high-temperature underdense plasma, laser energy is deposited near the critical density of the plasma and transferred to the ablation front by superthermal electrons, driving the implosion via the rocket effect. Transferring a higher portion of laser energy into the kinetic energy of the imploding shell, referred to as implosion efficiency, is pursued to relax the restriction on drive laser energy. The dependence of the implosion efficiency on laser absorption [2], laser-plasma instabilities, such as cross-beam energy transfer (CEBT) [3] and ablator material [4] have been investigated in direct-drive implosion experiments at the Omega laser facility.

Electron heat flux inhibition [5–8] induced by nonlocal electron transport also constrains the implosion efficiency. Efficient ablation requires electrons carrying heat flux from the critical surface to deposit all their energy in the conduction zone before they reach the ablation front. In ICF implosion, a higher drive laser intensity could, in principle, deposit more energy at the critical density and generate more electrons with higher mean energies. However, electrons with very high energies will have longer mean free paths and deposit their energies beyond the conduction zone, contributing less to the implosion. At drive laser intensity close to or greater than 10^{15} W/cm², the electron mean free path [$\lambda_e = \frac{3}{4(2\pi)^{1/2}} \frac{(kT_e)^2}{Zn_e e^4 \ln \Lambda}$] can reach several tens of micrometers. In this situation, the time needed to form a steady conduction zone is as long as several nanoseconds [9]. Consequently, the length of conduction zone D_c in units of λ_e might be quite small during the ablation process especially in the early

stage. Under this condition, the Fokker-Planck simulations [5,10,11] predict a much smaller electron heat flux than that predicted by the Spitzer-Harm (SH) model [12]. This implies a significant reduction in implosion efficiency from nonlocal electron transport at high drive laser intensities. Therefore, it is necessary to consider this effect when designing the pulse shape in direct-drive implosion experiments especially for those with ignition-scale drive lasers [13,14].

In this Letter, we investigated the elimination of electron heat flux inhibition by optimizing the main drive pulse design. Implosion efficiency dependency on the main drive pulse shape was studied experimentally. By applying a tailored double-gradient drive pulse in planar direct-drive experiments with a peak laser intensity over 10^{15} W/cm², the ablation depth and implosion velocity can be greatly enhanced compared to a square drive pulse with the same intensity. This cannot be explained by the common flux-limited SH model without considering the matching between electron mean free path and conduction zone length. Our Letter suggests that the peak intensity and temporal gradient of the main drive pulse are both important in efficient coupling of the laser energy to the ablation front under direct-drive conditions relevant to ignition-scale drive lasers.

Four laser beams from the SGII-Upgrade laser facility were used with up to 6-kJ total energy at 351-nm wavelength in a several nanosecond duration pulse. The laser beams irradiated CH foil targets at 50° relative to the normal axis of the targets. Continuous phase plates were applied to each beam to provide a smoothed quasi-Gaussian focal spot with 450- μ m diameter. The laser intensity on the targets could be varied from 3×10^{14} to 5×10^{15} W/cm², which is relevant to direct-drive fusion experiments. The ablation depth, which determines the remaining mass of the compressed shell, is an important parameter for direct-driven implosions. The burn-through depth

*jzhang1@sjtu.edu.cn

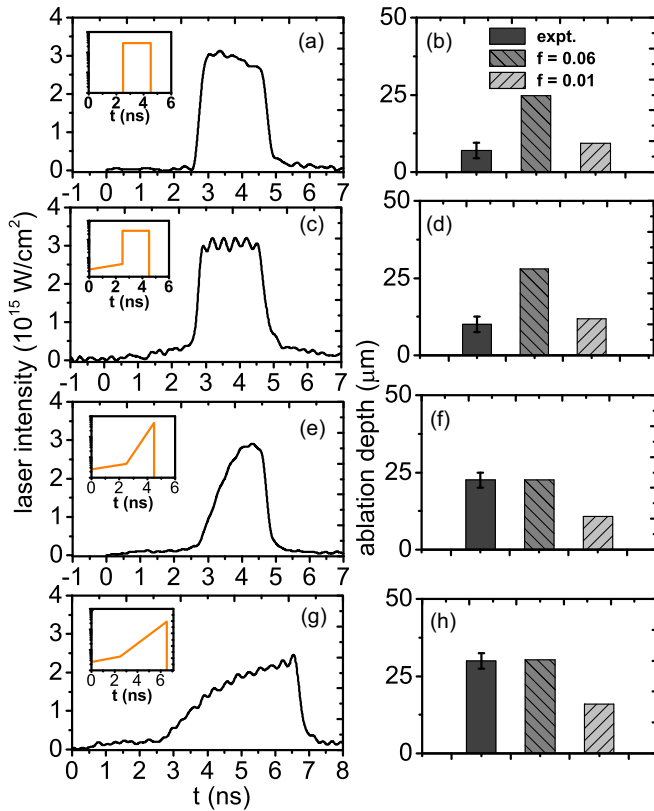


FIG. 1. (a), (c), (e), and (g) show the measured drive laser pulse shape and the designed pulse shape (inset) used in the experiments. (b), (d), (f), and (h) show ablation depths measured in the experiment (expt.) and simulated using the flux-limited SH model with constant flux limiters of $f = 0.06$ and $f = 0.01$.

method [2,7,13] was used to measure the ablation depth of the main drive pulse. The CH foil target had a 200-nm buried tracer layer of Ti. As Ti is ablated into the hot corona, a significant fraction of its population is ionized to the He and H-like charge states and emits K -shell emission. A flat Bragg crystal x-ray spectrometer was used to measure the He-like Ti resonance lines at 4.75 keV. Further details about the diagnosing methods used in the experiment are introduced in the Supplemental Material [15]. A range of ablation depths could be determined by changing the depth of the Ti layer in the CH foil target. Figure 1 shows the measured ablation depths for four different pulse shapes.

A standard drive pulse for ICF implosions consists of a prepulse with a small fraction of the drive laser energy to set an adiabat for the following implosion, whereas the main drive pulse with the remaining energy executes the implosion via the ablation process. A 2-ns square pulse with a peak laser intensity $\sim 3 \times 10^{15} \text{ W/cm}^2$ was the first main drive pulse used. The ablation depth of the pulse was measured to be $7.5 \pm 2.5 \mu\text{m}$. For comparison with the experimental results, simulations were conducted for each pulse shape using the MULTI code [14] with flux limiters f of 0.06 and 0.01. The simulated ablation depth for the sole square pulse case was $9.4 \mu\text{m}$ with a flux limiter of 0.01, which is quite close to the measured value. However, the simulated ablation depth was $24.7 \mu\text{m}$ with commonly used $f = 0.06$, which is much

larger than the experimental result. This clearly suggests a significant heat flux reduction for the square drive pulse at this intensity. To study whether the increased coronal plasma scale by the prepulse can mitigate the flux inhibition effect for the square main pulse, a 2.5-ns gradient prepulse with a laser intensity from $\sim 2.5 \times 10^{13}$ to $\sim 4.75 \times 10^{13} \text{ W/cm}^2$ was added before the square main pulse as shown in Fig. 1(c). The measured ablation depth for this pulse shape was $10 \pm 2.5 \mu\text{m}$. The simulated ablation depth using $f = 0.01$ was $11.9 \mu\text{m}$, whereas the simulation with $f = 0.06$ again gives a much larger value. Therefore, the prepulse had little effect on the ablation efficiency of the main drive pulse in our experiment, and the square main pulse was responsible for the significant heat flux inhibition and low mass ablation rate.

After the prepulse, the laser intensity on target is transitioned to the main drive pulse in a time of dt . The transition speed can be characterized by the intensity gradient dI/dt of the main drive pulse. The intensity gradient dI/dt for the square pulse used in the experiment was $\sim 5.5 \times 10^{15} \text{ W/(cm}^2\text{ns)}$. To further study the role of the intensity gradient of the main drive pulse, the square main drive pulse was replaced by a 2-ns gradient drive pulse with a peak intensity of $\sim 3 \times 10^{15} \text{ W/cm}^2$ and dI/dt of $\sim 2.1 \times 10^{15} \text{ W/(cm}^2\text{ns)}$ as shown in FIG. 1(e). The measured ablation depth significantly increased to $22.5 \pm 2.5 \mu\text{m}$. In comparison, the simulated ablation depths for the pulse shape were 22.6 and $10.8 \mu\text{m}$ with $f = 0.06$ and $f = 0.01$, respectively, as shown in Fig. 1(f). This indicates a significantly more efficient ablation for the double-gradient pulse than the square pulse. As shown in Fig. 1(g), when the gradient for the main drive pulse was further decreased to $\sim 6 \times 10^{14} \text{ W/(cm}^2\text{ns)}$ as the laser intensity increased from $\sim 4.75 \times 10^{13}$ to $\sim 2.4 \times 10^{15} \text{ W/cm}^2$ in ~ 4 ns, an increased ablation depth of $30.0 \pm 2.5 \mu\text{m}$ was measured. And simulations with $f = 0.06$ successfully reproduced the measured ablation depth as well.

In addition to the remaining mass, the velocity of the compressed target accelerated via rocket effect also reflects the implosion efficiency. In our experiment, the implosion velocity was characterized by the ablation front trajectory, which was obtained from the temporally and spatially resolved x-ray bremsstrahlung from the laser-driven CH target. The ablation front position was located close to the point at which where the x-ray intensity experienced a sharp decrease. Similar techniques have been applied in diagnosing implosion dynamics in Omega's direct-drive experiments [4,16–18]. The velocity of the ablation front was also found to be strongly dependent on the intensity gradient in our experiment. The gradients of the 5.8-kJ square pulse and 5.0-, 3.6-, and 2.3-kJ double-gradient pulses were $\sim 5.5 \times 10^{15}$, $\sim 2.1 \times 10^{15}$, $\sim 1.5 \times 10^{15}$, and $\sim 9.6 \times 10^{14} \text{ W/(cm}^2\text{ns)}$, respectively. As shown in Fig. 2(b), for the double-gradient pulse, the ablation surface velocity increased as the laser energy increased. During the first 2.5 ns, the average ablation surface velocity was approximately 12 km/s, which slightly increased as the laser energy increased. The ablation surface acceleration was mainly contributed by the main gradient pulse. The averaged velocities in the latter 2.5 ns were approximately 75, 102, and 175 km/s, respectively, for the three double-gradient pulses. However, for the 2-ns square pulse with a gradient of $\sim 5.5 \times 10^{15} \text{ W/(cm}^2\text{ns)}$, the velocity of the ablation front

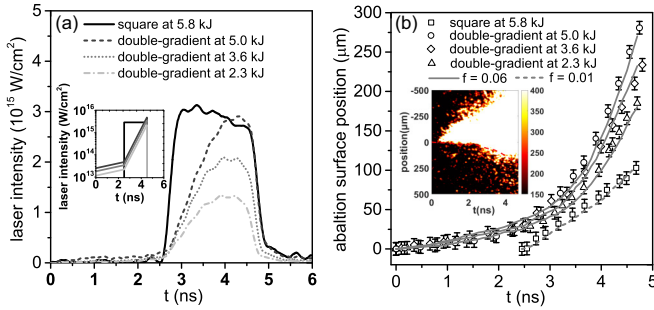


FIG. 2. (a) Drive laser pulses used in the experiment, including square pulse with drive energy of 5.8 kJ (solid black) and double-gradient pulses of 5.0, 3.6, and 2.3 kJ. The inset is the designed shape of these pulses. (b) Measured and simulated ablation surface trajectories for the drive pulses in (a) with $f = 0.06$ (solid gray line) and $f = 0.01$ (dashed gray line), respectively. The targets used in these shots are 50- μm -thick planar CH foil. The inset is the typical time and space-resolved x-ray self-emission profile from laser-ablated CH target driven by double-gradient pulse of 5.0 kJ. The red dashed line represents the inferred ablation surface trajectory.

was quite low at only ~ 56 km/s. Hydrodynamic simulations suggest a flux limiter of 0.06 for the double-gradient pulses whereas 0.01 for the square pulse. Compared to the square pulse, the ablated mass was enhanced by 200%, and the ablation front velocity increased by 210%. Consequently, the kinetic energy of the imploded target was enhanced by a factor of ~ 6 . This clearly suggests that a large gradient of the main drive pulse may result in significant reduction of heat flux and implosion efficiency.

Apart from the diminished implosion efficiency, a secondary effect of the significant heat flux inhibition owing to the large gradient is the reduced energy absorption fraction at the critical surface [13]. In the experiment, several laser energy meters were set in different directions to measure the scattered energy to provide a rough estimation of the scattered energy portion for different pulse shapes. In addition, the plasma density scale length was inferred from the spatial distribution of the continuous bremsstrahlung radiation provided by a Bragg crystal spectrometer. As shown in Fig. 3(a), the typical scale length for a double-gradient pulse was ~ 240 μm , whereas it was only ~ 170 μm for the square pulse. The small scale length might result in an inefficient inverse-bremsstrahlung absorption process. The scattered energy portion for the square pulse was 12.7%, which is ~ 5.5 times that for the double-gradient pulse of 5.0 kJ. For the square pulse, the scattered energy was mainly from the laser backscatter direction. This indicates that a strong reflection may occur near the critical surface owing to the small scale length. It should be noted the large scale length for the double-gradient pulse might be disadvantageous, which could result in the birth and growth of laser-plasma instabilities, such as the stimulated Raman scattering and CEBT. However, this disadvantage seems a minor effect in our experiment compared to the significant increase of the implosion efficiency.

Our experimental results indicate that the intensity gradient plays a significant role in the energy-coupling process between the critical and the ablation surfaces. In principle, the intensity gradient influences the evolution of the conduction

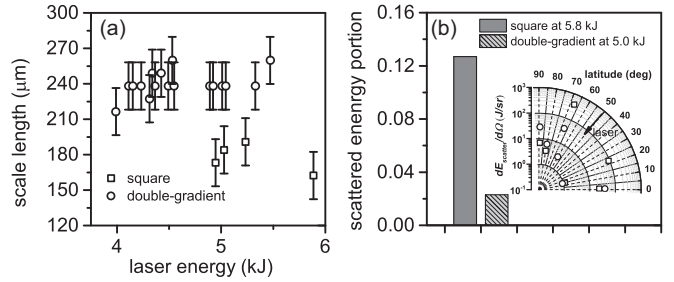


FIG. 3. (a) Measured density scale length of the coronal plasmas for the square and double-gradient pulses. (b) Measured scattered laser energy portion for the square pulse of 5.8 kJ and the double-gradient pulse of 5.0 kJ. The inset is the angular distribution of scattered laser energy in the experiment. The results for square and double-gradient pulses are displayed with open squares and circles, respectively.

zone size and the electron mean free path, which determines the simultaneous nonlocality of the electron heat flux. It is still an open question how to properly address this effect to the hydrodynamic simulation of the electron heat transport process [19]. Epperlein and Short [5,10] proposed an analytical flux limiter model to account for heat flux inhibition due to nonlocal electron transport in a temperature perturbation. For electron transport in the conduction zone, the flux limiter f can be expressed as

$$f(t) = 1 / \{1 + \alpha [\lambda_e(t) / D_c(t)]^2\}, \quad (1)$$

where α is an adjustable parameter. With this formula, a constant flux limiter in the flux-limited SH model is replaced with a time-dependent limiter to follow the evolution of the electron mean free path and conduction zone length. Similar models have been applied to simulate the electron thermal conduction process in laser direct-drive implosions [8,20]. Simulations with this time-dependent electron thermal conduction model well reproduced all the ablation depths and ablation front trajectory for the various pulse shapes in our experiment, when the adjustable parameter α was 5.0. The evolution of the ratio D_c / λ_e for the square and double-gradient main drive pulses were investigated using the time-dependent flux-limited SH model shown in Fig. 4(b). For the double-gradient pulse, however, the ratio λ_e / D_c was ~ 7 , resulting in $\sim 50\%$ of the laser intensity being converted into local electron heat flux. This suggests that a moderate intensity gradient gives the conduction zone more time to expand so that it can adapt to a large electron mean free path at higher laser intensities.

We further investigated the peak intensity and gradient threshold for an efficient direct-drive ablation process by comparing simulation results using the flux-limited SH model with $f = 0.06$ and the time-dependent electron heat flux-limited model, respectively, as shown in Figs. 4(c) and 4(d). When the peak laser intensity was below $\sim 7.5 \times 10^{14}$ W/cm², the ablation depths obtained using the time-dependent flux limiter agreed well with the widely used $f = 0.06$. However, the ablation depth significantly as the peak laser intensity exceeds $\sim 7.5 \times 10^{14}$ W/cm², indicating a significant electron heat flow reduction at higher laser intensities. When peak drive laser

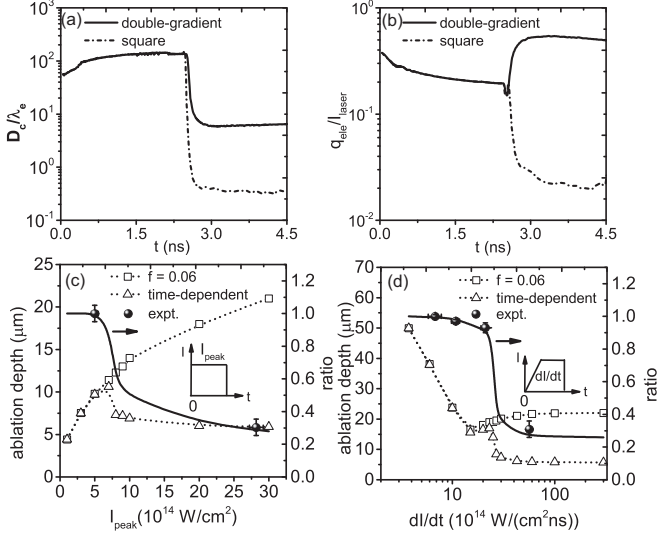


FIG. 4. Evolution of (a) the ratios D_c/λ_e and (b) q_{ele}/I_{abs} for the double-gradient and the square pulses used in the experiment. Dependence of the simulated ablation depth using $f = 0.06$ (open square) and the time-dependent flux limiter model (open triangle) on (c) the peak laser intensity of a 2-ns square pulse and (d) the intensity gradient for a single-gradient pulse with peak intensity of $\sim 3 \times 10^{15} \text{ W/cm}^2$. The solid line represents the ratio between the two simulated ablation depths by the time-dependent flux limiter model and $f = 0.06$, respectively. And the experimental value (black sphere) is also displayed.

intensity exceeded the threshold, the role of laser intensity gradient became significant. By varying the gradient of the pulse, a threshold of $\sim 2.5 \times 10^{15} \text{ W}/(\text{cm}^2 \text{ ns})$ for the temporal gradient was found as shown in Fig. 4(d). When the gradient exceeded the threshold, the heat flux was significantly reduced. This is because the increase in the electron mean free path is much faster than the expansion of the conduction zone length, resulting in an increased mismatch between the electron mean free path and the conduction zone length during the ablation process. It can be concluded that the temporal gradient should be limited to below $\sim 2.5 \times 10^{15} \text{ W}/(\text{cm}^2 \text{ ns})$ for the main drive pulse of direct-drive implosion as the peak laser intensity is greater than $\sim 7.5 \times 10^{14} \text{ W}/(\text{cm}^2 \text{ ns})$.

Another important insight from this simple model is that the flux inhibition level can be maintained at a minimum if the conduction zone length is more than \sim ten times the electron mean free path [10]. This condition can be satisfied if the conduction zone expansion speed exceeds ten times the electron mean free path increase, which can be expressed as

$$\frac{dD_c}{dt} \gtrsim R d\lambda_e/dt. \quad (2)$$

Based on stationary ablation theory [9], a critical gradient can also be analytically derived as (see the Supplemental Material [15] for further details),

$$dI_{14}/dt [10^{14} \text{ W}/(\text{cm}^2 \text{ ns})] \lesssim 30(A/2Z)^{-1}. \quad (3)$$

For CH plasmas, the threshold is $\sim 3.2 \times 10^{15} \text{ W}/(\text{cm}^2 \text{ ns})$, which is close to that obtained from the above simulation with

the time-dependent flux limiter model. Traditionally, the main drive pulse gradient was mainly designed to adiabatically compress the shell in Omega's direct-drive experiments [21]. As the drive laser intensity increases, our Letter indicates the gradient not only affects the adiabatic compression, but also affects the electron thermal conduction process. The matching between the conduction zone and the electron mean free path is usually satisfied in cases with peak laser intensity of several 10^{14} W/cm^2 . This is because of both the smaller λ_e and the shorter time required to form a conduction zone with sufficient width under this condition. However, when the drive laser intensity is great than 10^{15} W/cm^2 , for ignition-scale direct-drive implosions, such as the polar-drive scheme [22], the required time to reach a steady state becomes several nanoseconds, and λ_e can reach a few tens of micrometers. As a result, severe electron heat flux inhibition might occur if the gradient is not moderate enough. Compared with the conduction zone, the electron mean free path is much more sensitive to the increased laser intensity. Consequently, the temporal gradient of the main drive pulse must be limited to maintain D_c/λ_e with a relatively large value. Our Letter suggests a proper gradient is the key to eliminate the heat flux inhibition effect for direct-drive implosions featuring with laser intensity over 10^{15} W/cm^2 . In addition, our findings about the laser pulse gradient can be potentially applied to the shock ignition scheme. The ignition is achieved by a strong shock with pressure of 200–300 Mbar driven by a picket pulse with an on-target intensity of $5\text{--}10 \times 10^{15} \text{ W/cm}^2$. However, the measured pressure is 20%–50% lower than the prediction from the stationary ablation theory [23]. This is partially explained by the reduced laser absorption due to laser plasma interaction instabilities, such as CEBT [3]. In the experiment, the laser intensity on target increases from $\sim 5 \times 10^{14}$ to $\sim 1.2 \times 10^{15} \text{ W/cm}^2$ in $\sim 0.2 \text{ ns}$, corresponding a temporal gradient of $\sim 3.5 \times 10^{15} \text{ W}/(\text{cm}^2 \text{ ns})$, which exceeds the gradient threshold. Therefore, the electron heat flux inhibition from the large picket pulse gradient may be another possible reason for the ablation pressure being lower than predicted. Our Letter suggests a gradient leading edge might be necessary for the picket pulse to convert the peak laser intensity into the designed ablation pressure effectively.

In conclusion, we demonstrated the critical role of the intensity gradient in coupling laser energy to the ablation front in direct-drive implosion experiments with laser intensities over 10^{15} W/cm^2 . Compared to the square drive pulse, the ablation depth, ablation front velocity and implosion efficiency can be significantly increased with a tailored double-gradient drive pulse. The enhancement is caused by a moderate gradient that helps match the electron mean free path and the corresponding conduction zone length, which relieves the heat flux inhibition by the nonlocal electron transport. With the conduction zone length maintained at more than \sim ten times the electron mean free path, the laser energy at the critical surface can be efficiently converted into the local electron heat flux, ensuring efficient ablation. Simulations using a time-dependent flux-limited SH model indicates the gradient should be no more than $\sim 2.5 \times 10^{15} \text{ W}/(\text{cm}^2 \text{ ns})$ when the peak intensity of the main drive pulse is over $\sim 7.5 \times 10^{14} \text{ W/cm}^2$. These results validate

the significant importance of pulse shape design in ignition-scale laser direct-drive implosion experiments.

We thank the SG-IIU technical staff at the Shanghai Institute of Optics and Fine Mechanics for their support during the

experiments. This work was supported by the Strategic Priority Research Program of the Chinese Academy of Sciences (Grants No. XDA25010000, No. XDA25030000, and No. XDA25050200) and the National Natural Science Foundation of China (Grant No. 12105173).

- [1] R. Betti and O. A. Hurricane, *Nat. Phys.* **12**, 435 (2016).
- [2] S. P. Regan, R. Epstein, V. N. Goncharov, I. V. Igumenshchev, D. Li, P. B. Radha, H. Sawada, W. Seka, T. R. Boehly, J. A. Delettrez, O. V. Gotchev, J. P. Knauer, J. A. Marozas, F. J. Marshall, R. L. McCrory, P. W. McKenty, D. D. Meyerhofer, T. C. Sangster, D. Shvarts, S. Skupsky, V. A. Smalyuk, B. Yaakobi, and R. C. Mancini, *Phys. Plasmas* **14**, 056305 (2007).
- [3] D. H. Froula, I. V. Igumenshchev, D. T. Michel, D. H. Edgell, R. Follett, V. Y. Glebov, V. N. Goncharov, J. Kwiatkowski, F. J. Marshall, P. B. Radha, W. Seka, C. Sorce, S. Stagnitto, C. Stoeckl, and T. C. Sangster, *Phys. Rev. Lett.* **108**, 125003 (2012).
- [4] D. T. Michel, V. N. Goncharov, I. V. Igumenshchev, R. Epstein, and D. H. Froula, *Phys. Rev. Lett.* **111**, 245005 (2013).
- [5] E. M. Epperlein and R. W. Short, *Phys. Rev. E* **50**, 1697 (1994).
- [6] R. J. Henchen, M. Sherlock, W. Rozmus, J. Katz, D. Cao, J. P. Palastro, and D. H. Froula, *Phys. Rev. Lett.* **121**, 125001 (2018).
- [7] G. Schurtz, S. Gary, S. Hulin, C. Chenais-Popovics, J. C. Gauthier, F. Thais, J. Breil, F. Durut, J. L. Feugeas, P. H. Maire, P. Nicolai, O. Peyrusse, C. Reverdin, G. Soullie, V. Tikhonchuk, B. Villette, and C. Fourment, *Phys. Rev. Lett.* **98**, 095002 (2007).
- [8] S. X. Hu, V. A. Smalyuk, V. N. Goncharov, S. Skupsky, T. C. Sangster, D. D. Meyerhofer, and D. Shvarts, *Phys. Rev. Lett.* **101**, 055002 (2008).
- [9] R. Fabbro, C. Max, and E. Fabre, *Phys. Fluids* **28**, 1463 (1985).
- [10] E. M. Epperlein and R. W. Short, *Phys. Fluids B* **3**, 3092 (1991).
- [11] A. Marocchino, M. Tzoufras, S. Atzeni, A. Schiavi, P. D. Nicolai, J. Mallet, V. Tikhonchuk, and J. L. Feugeas, *Phys. Plasmas* **20**, 977 (2013).
- [12] L. Spitzer and R. Härm, *Phys. Rev.* **89**, 977 (1953).
- [13] J. Delettrez, *Can. J. Phys.* **64**, 932 (1986).
- [14] R. Ramis and J. Meyer-ter-Vehn, *Comput. Phys. Commun.* **203**, 226 (2016).
- [15] See Supplemental Material at <http://link.aps.org/supplemental/10.1103/PhysRevE.105.L053203> for the diagnosing techniques used in the experiment and mathematical derivations for the intensity gradient threshold.
- [16] D. T. Michel, C. Sorce, R. Epstein, N. Whiting, I. V. Igumenshchev, R. Jungquist, and D. H. Froula, *Rev. Sci. Instrum.* **83**, 10E530 (2012).
- [17] D. T. Michel, A. K. Davis, W. Armstrong, R. Bahr, R. Epstein, V. N. Goncharov, M. Hohenberger, I. V. Igumenshchev, R. Jungquist, D. D. Meyerhofer, P. B. Radha, T. C. Sangster, C. Sorce, and D. H. Froula, *High Power Laser Sci. Eng.* **3**, e19 (2015).
- [18] D. T. Michel, A. K. Davis, V. N. Goncharov, T. C. Sangster, S. X. Hu, I. V. Igumenshchev, D. D. Meyerhofer, W. Seka, and D. H. Froula, *Phys. Rev. Lett.* **114**, 155002 (2015).
- [19] S. Lebedev, *Plasma Phys. Controlled Fusion* **46**, 1805 (2004).
- [20] A. Sunahara, J. A. Delettrez, C. Stoeckl, R. W. Short, and S. Skupsky, *Phys. Rev. Lett.* **91**, 095003 (2003).
- [21] V. Gopalaswamy, R. Betti, J. P. Knauer, N. Luciani, D. Patel, K. M. Woo, A. Bose, I. V. Igumenshchev, E. M. Campbell, K. S. Anderson, K. A. Bauer, M. J. Bonino, D. Cao, A. R. Christopherson, G. W. Collins, T. J. B. Collins, J. R. Davies, J. A. Delettrez, D. H. Edgell, R. Epstein, C. J. Forrest, D. H. Froula, V. Y. Glebov, V. N. Goncharov, D. R. Harding, S. X. Hu, D. W. Jacobs-Perkins, R. T. Janezic, J. H. Kelly, O. M. Mannion, A. Maximov, F. J. Marshall, D. T. Michel, S. Miller, S. F. B. Morse, J. Palastro, J. Peebles, P. B. Radha, S. P. Regan, S. Sampat, T. C. Sangster, A. B. Sefkow, W. Seka, R. C. Shah, W. T. Shmyada, A. Shvydky, C. Stoeckl, A. A. Solodov, W. Theobald, J. D. Zuegel, M. G. Johnson, R. D. Petrasso, C. K. Li, and J. A. Frenje, *Nature (London)* **565**, 581 (2019).
- [22] M. Hohenberger, P. B. Radha, J. F. Myatt, S. LePape, J. A. Marozas, F. J. Marshall, D. T. Michel, S. P. Regan, W. Seka, A. Shvydky, T. C. Sangster, J. W. Bates, R. Betti, T. R. Boehly, M. J. Bonino, D. T. Casey, T. J. B. Collins, R. S. Craxton, J. A. Delettrez, D. H. Edgell, R. Epstein, G. Fiksel, P. Fitzsimmons, J. A. Frenje, D. H. Froula, V. N. Goncharov, D. R. Harding, D. H. Kalantar, M. Karasik, T. J. Kessler, J. D. Kilkenny, J. P. Knauer, C. Kurz, M. Lafon, K. N. LaFortune, B. J. MacGowan, A. J. Mackinnon, A. G. MacPhee, R. L. McCrory, P. W. McKenty, J. F. Meeker, D. D. Meyerhofer, S. R. Nagel, A. Nikroo, S. Obenshain, R. D. Petrasso, J. E. Ralph, H. G. Rinderknecht, M. J. Rosenberg, A. J. Schmitt, R. J. Wallace, J. Weaver, C. Widmayer, S. Skupsky, A. A. Solodov, C. Stoeckl, B. Yaakobi, and J. D. Zuegel, *Phys. Plasmas* **22**, 056308 (2015).
- [23] M. Hohenberger, W. Theobald, S. X. Hu, K. S. Anderson, R. Betti, T. R. Boehly, A. Casner, D. E. Fratanduono, M. Lafon, D. D. Meyerhofer, R. Nora, X. Ribeyre, T. C. Sangster, G. Schurtz, W. Seka, C. Stoeckl, and B. Yaakobi, *Phys. Plasmas* **21**, 022702 (2014).